Effects of in-medium *NN* cross section and density distribution on the reaction cross sections of Ne, Mg, and O isotopes with ^{12}C at 1 GeV

M. Rashdan and Sh. Sewailem
Department of Mathematics and Theoretical Physics, AEA, Cairo, Egypt

(Received 11 November 2018; published 6 March 2019)

The nucleus-nucleus reaction cross sections of $^{18-34}$Ne, $^{20-36}$Mg, $^{16-24}$O + ^{12}C at one GeV/u are calculated in the Glauber theory using different models of the nucleon-nucleon (*NN*) cross sections and nuclear densities. For in-medium effects, we consider the phenomenological (Ph), geometrical Pauli (GP), and modified combined (MC) models for the *NN* reaction cross section. For the density distributions, we used the Sao Paulo (SP), Skyrme-Hartree-Fock (SHF), and the angle-averaged deformed Fermi (DF) densities. The results are compared with experiments as well as other theoretical calculations. It is found that the data can, generally, be described by using the Ph and GP models for in-medium effects with the SP density, which, on the other hand, predicted smaller radii. A satisfactory explanation of the experimental data is obtained by using more realistic densities such as SHF and DF with realistic radii, and the MC model for medium modifications, which involve the combined effect of the phase variation, higher momentum transfer components, and Pauli blocking of the *NN* amplitude. The in-medium Ph and GP models when used with realistic densities, cannot describe the data at 1 GeV.

DOI: 10.1103/PhysRevC.99.034604

I. INTRODUCTION

In recent years, great effort and progress has been made for studying the structure and reactions of nuclei far from the β stability line, on both the theoretical and experimental sides [1–10]. Horiuchi *et al.* [11] calculated the reaction cross sections of Ne, Mg, Si, O + ^{12}C at intermediate and high energies, using the Glauber model with the angle-averaged deformed SHF densities with neglecting medium effects. The calculated total reaction cross sections consistently agree with the cross section data on Ne + ^{12}C at 240 MeV/u. However, considerable disagreement between the calculated and the measured cross sections for O, Ne, and Mg isotopes on a ^{12}C target at around one GeV/u has been observed. The resolution of these problems requires further investigations in both theory and experiment, as they have been concluded there. Panda *et al.* [12] have used the Glauber model with the relativistic mean-field (RMF) densities to calculate the nucleus-nucleus reaction cross sections of these systems at intermediate and high energies using the Glauber model with neglecting medium modifications. The reaction cross section calculated at 1 GeV strongly overestimated the data. Sharma *et al.* [13] calculated the reaction cross sections at about 1 GeV in the framework of the Glauber model using RMF and SHF densities also with neglecting medium effects on the *NN* cross section as Horiuchi *et al.* and Panda *et al.* Again the calculated nucleus-nucleus reaction cross sections overestimated the data. For example, for ^{20}O + ^{12}C the spherical and deformed RMF densities calculated using NL3 interaction, which predicted closer values to the experimental data than the other used RMF parameterizations, overestimated the data by about 50 and 100 mb when using spherical and deformed densities. The largest reaction cross section has been obtained by the SHF density, with SEI-I interaction, which much more overestimated the data by 160 mb (see Table II and Fig. 4 of Ref. [13]).

In a previous work [14] the total reaction cross sections of Ne and Mg isotopes colliding by ^{12}C at 240 MeV/u have been analyzed using the Dirac-Brueckner approach (DBA) [15–22] and Glauber model, where consistency description of the data has been obtained. In DBA, the Dirac-Brueckner-Bethe-Goldstone equation is solved, locally, in momentum space configuration of two colliding nuclear matters, starting from the one-boson-exchange potential of Bonn [23] as a bare *NN* interaction. This procedure yields a complex interaction energy and consequently complex optical potentials, which have been used to calculate the reaction cross sections of $^{20-36}$Ne, $^{24-38}$Mg + ^{12}C at 240 MeV/u. Medium modifications are fully incorporated in this relativistic microscopic approach through the Pauli operator, the modifications of the Dirac spinors of the single-particle Hamiltonian in the nuclear medium and the density-dependent effective nucleon mass. However, the application of this approach for calculating the optical potential is, normally, limited to intermediate energy below the pion threshold (∼300 MeV) [24–26], due to difficulties arising from the opening of inelastic channels such as those associated with pion production or Δ resonances.

The Glauber model, which can be applied for intermediate and high energies, has also been used in our previous calculations [14] of the reaction cross sections of Ne and Mg isotopes on a ^{12}C at 240 MeV/u. Different models for in-medium modifications such as the DBA parametrization (DBAP) [27,28], the phenomenological model [29] and the geometrical Pauli model [30] have been investigated. The DBAP is a parametrization of the in-medium *NN* cross section

based on the Dirac-Brueckner approach. The Ph model is a modification of the DBA parametrization, which consisted in combining the free NN cross sections parametrized in Ref. [31] with the Brueckner theory results of Refs. [27,28]. In the GP model, introduced by Karakoc and Bertulani [30], in-medium effects on the NN reaction cross section are included by calculating Pauli projection operator, appearing in the G matrix. It has been found that the Glauber model satisfactorily described the data at 240 MeV/u when using the phenomenological model as well as the geometrical Pauli model for the in-medium effects and the realistic SHF densities. From this result of our earlier work at 240 MeV/u [14] and on the calculations of Refs. [11–13] at 1 GeV/u important questions arise. Why may one expect that the Glauber model should not apply to higher energetic nuclear reactions? Do the in-medium modifications in the cross sections make the difference between lower and higher energies or between the density distributions of the nuclei? We would expect that the in-medium modifications are the crucial task here. Thus it is interesting to investigate the effect of medium modifications models for the case of high-energy nuclear collisions around 1 GeV/u.

The aim of the present work is to extend our earlier work at 240 MeV/u [14] to high energy around 1 GeV/u. We used different models for the density distributions, as well as medium modifications. For medium modifications, we consider three different models; the phenomenological, geometrical Pauli blocking and modified combined [32], which involve combined effect arising due to phase variation, higher momentum transfer components, and Pauli blocking. For the density distributions, we consider the Sao Paulo [33], Skyrme-Hartree-Fock [34–36], and deformed Fermi density models. These models for in-medium effects and density distributions will be discussed in detail in Sec. II. Section III presents results and discussion. A summary and conclusion are presented in Sec. IV.

II. THEORETICAL DESCRIPTION

The nucleus-nucleus reaction cross section in the optical limit of the Glauber model can be written, as

$$\sigma_R = 2\pi \int_0^\infty db\, b[1 - e^{-\chi(b)}]. \tag{1}$$

where,

$$\chi(b) = \int dZ \int d^3r\, \overline{\sigma}_{NN}(E,\rho)\rho_P(|\,\mathbf{r} - \mathbf{R}\,|)\rho_T(\mathbf{r}). \tag{2}$$

The vector $\mathbf{R}$ is the line joining the centers of the two colliding nuclei, where $R = \sqrt{b^2 + Z^2}$ and b is the impact parameter. ρ_T and ρ_P are the target and projectile densities and $\overline{\sigma}_{NN}[E, \rho = \rho_T(\mathbf{r}) + \rho_P(|\mathbf{r} - \mathbf{R}|)]$ is the isospin averaged nucleon-nucleon (NN) cross section, which depends on the density of the two interacting nuclei and incident energy. The functional form of this dependence can be written as [29],

$$\overline{\sigma}_{NN}(E,\rho) = \frac{N_P N_T \sigma^*_{nn} + Z_P Z_T \sigma^*_{pp} + (N_P Z_T + N_T Z_P)\sigma^*_{np}}{A_P A_T}, \tag{3}$$

where Z_i, N_i, and A_i ($i = T$ or P) are the proton, neutron, and mass number of the nucleus i. It may be noted that Eq. (1) gives the reaction cross section, σ_R, which also includes any inelastic cross section to bound excited states of the projectile and target, while the measured is the interaction cross section σ_I, $\sigma_R = \sigma_I + \sigma_{\rm inel}$. The difference between σ_R and σ_I is estimated and it was found to be at most 100 mb in a phenomenological way [37]. This difference is expected to be smaller as it goes closer to the neutron drip line, since the inelastic cross sections are expected to be small because they are much more weakly bound. Hence σ_R can be approximated to σ_I [38]. The assumption $\sigma_R \backsimeq \sigma_I$ has been examined in Ref. [38] for the Carbon isotopes for energy around 280 MeV/u colliding with ^{12}C and it has been found to be quantified and validated where the sum of the inelastic cross sections of the target and projectile has been found to be smaller than the uncertainty on the interaction cross section. A similar conclusion has been found for magnesium isotopes for energies around 250 MeV/u [39]. Furthermore, at relativistic energies, $\sigma_{\rm inel}$ is smaller than the typical errors of σ_I and, therefore, σ_I can be assumed to be nearly equal to σ_R. Hence, the Glauber model, Eq. (1), can be used to calculate both σ_I and σ_R [32]. We use this approximation, which has been used in Ref. [32] as well as by many other authors (see, for example, Refs. [11–14,38–42]).

The in-medium NN cross sections, appearing in Eq. (3), are assumed to be factorized as the product of a medium correction factor $F(E,\rho)$ and the free NN cross sections [14,43], which reads

$$\sigma^*_{NN}(E,\rho_P,\rho_T) = \sigma^{\rm Free}_{NN}(E) \times F_{NN}(E,\rho). \tag{4}$$

In the following we discuss three different parametrization models for including in-medium effects in the NN reaction cross sections.

A. Medium modifications models

The first model is the phenomenological model, which is widely used in the literature [5,14,29,44–46] for including in-medium effects on the NN cross sections, which can be written as

$$\sigma^*_{pp}(E;\rho) = \sigma^{\rm free}_{pp}(E) \times F_{pp}(E,\rho), \tag{5}$$

$$\sigma^*_{nn}(E;\rho) = \sigma^*_{pp}(E;\rho). \tag{6}$$

$$\sigma^*_{np}(E;\rho) = \sigma^{\rm free}_{np}(E) \times F_{np}(E,\rho), \tag{7}$$

where, the free NN cross sections can be written as (in mb units),

$$\begin{aligned}\sigma^{\rm free}_{pp}(E) &= \sigma^{\rm free}_{nn}(E)\\ &= 13.73 - 15.04(v/c)^{-1}\\ &\quad + 8.76(v/c)^{-2} + 68.67(v/c)^4,\end{aligned} \tag{8}$$

$$\begin{aligned}\sigma^{\rm free}_{np}(E) &= -70.67 - 18.18(v/c)^{-1}\\ &\quad + 25.26(v/c)^{-2} + 113.85(v/c),\end{aligned} \tag{9}$$

where E is the energy per nucleon of the projectile and the velocity $v/c = \sqrt{1 - 1/\gamma^2}$, where $\gamma = \frac{E}{931.5} + 1$. The

density-dependent factors are given in this model by [29]

$$F_{pp}(E,\rho) = F_{nn}(E,\rho) = \frac{1+7.772E^{0.06}\rho^{1.48}}{1+18.01\rho^{1.46}}, \quad (10)$$

$$F_{np}(E,\rho) = \frac{1+20.88E^{0.04}\rho^{2.02}}{1+35.86\rho^{1.9}}. \quad (11)$$

The parameters of this phenomenological model are adjusted to reproduce the nucleus-nucleus reaction cross sections. The local density dependence of the *NN* cross section is used, where the density is taken as the sum of the target and projectile densities in each volume element being considered, i.e., the local density at each point along the trajectory.

The second parametrization model for including in-medium effects is the geometrical Pauli (GP) model, which was introduced by Karakoc and Bertulani [30]. In this model in-medium effects on the *NN* reaction cross sections are included by calculating Pauli projection operator, appearing in the *G* matrix. The functional form of the in-medium density-dependent factor F_{NN} is given by [30]

$$F_{NN}(E,\rho) = \frac{1}{1+1.892\left(\frac{2\rho_<}{\rho_0}\right)\left(\frac{|\rho_P-\rho_T|}{\widetilde{\rho}\rho_0}\right)^{2.75}} \times \begin{cases} 1-\frac{37.02\widetilde{\rho}^{2/3}}{E}, & \text{if } E > 46.27\widetilde{\rho}^{2/3} \\ \frac{E}{231.38\widetilde{\rho}^{2/3}}, & \text{if } E \leqslant 46.27\widetilde{\rho}^{2/3} \end{cases}, \quad (12)$$

where $\widetilde{\rho} = (\rho_P + \rho_T)/\rho_0$, $\rho_< = \min(\rho_P, \rho_T)$, and $\rho_0 = 0.17$ fm^{-3}. The free *NN* cross section of this model is given explicitly in Ref. [30], whose parameters fit the experimental *NN* data over a variety of energies, ranging from 10 MeV to 5 GeV.

The third model used for including medium modifications is the MC model, which has been described in detail by Ahmed *et al.* [32]. In this model, the in-medium *NN* amplitude has been modified to include combined effects arising due to phase variation, higher momentum transfer components, and Pauli blocking. Ahmed *et al.* used this MC model and they were able to describe in a satisfactory manner the O + C reaction cross section data at 1 GeV/u, using harmonic oscillator densities with realistic radii. Thus the model is expected to be more appropriate at high energy.

B. Density distribution models

For the proton and neutron density distributions of target and projectiles we first use the SP density provided by the Sao Pauli group [33] as a global density. The SP density has the functional form of the two-parameter Fermi, as

$$\rho_{p,n}(r) = \frac{\rho_0}{1+\exp\left(\frac{r-R_{0p,n}}{a_{0p,n}}\right)}, \quad (13)$$

where the parameters $R_{0p,n}$ and $a_{0p,n}$ are obtained in Ref. [33], as

$$R_{0p} = 1.81Z^{1/3} - 1.12, \quad a_{0p} = 0.47 - 0.00083Z \quad (14)$$

$$R_{0n} = 1.49N^{1/3} - 0.79, \quad {}_{0n} = 0.47 + 0.00046N, \quad (15)$$

where, Z and N are the proton and neutron number, respectively. It is worth mentioning that the SP density is fitted to the calculated results of the Dirac-Hartree-Bogoliubov model in the stable nuclear region. The results for the SP root-mean-square (rms) radii are listed in Tables I–III for Ne, Mg, and O isotopes.

TABLE I. rms radii for Ne isotopes predicted by the SP density distribution defined by Eqs. (13)–(15).

Nucleus	R_n(fm)	R_p(fm)	R_m(fm)
^{18}Ne	2.445	2.753	2.621
^{19}Ne	2.511	2.753	2.641
^{20}Ne	2.574	2.753	2.665
^{21}Ne	2.634	2.753	2.692
^{22}Ne	2.692	2.753	2.720
^{23}Ne	2.747	2.753	2.750
^{24}Ne	2.801	2.753	2.781
^{25}Ne	2.852	2.753	2.813
^{26}Ne	2.902	2.753	2.846
^{27}Ne	2.950	2.753	2.879
^{28}Ne	2.997	2.753	2.912
^{29}Ne	3.042	2.753	2.946
^{30}Ne	3.087	2.753	2.980
^{31}Ne	3.130	2.753	3.013
^{32}Ne	3.172	2.753	3.047

The second model for the nuclear density is the SHF [34,35], where we perform SHF calculation for both target and projectiles assuming spherical symmetry, adopting SKRA force [36], which seems to address the nuclear interactions adequately. The ground state is obtained by minimizing the energy density functional [34], $E(\rho) = E_N + E_C - E_{cm}$. The Coulomb energy E_C includes both direct and exchange parts. The center-of-mass energy E_{cm} is approximated by the usual approximation $E_{cm} \approx \sum_i p_i^2/(2mA)$. The nuclear energy E_N is given by a functional of the nucleon density $\rho_q(\mathbf{r})$, the kinetic density $\tau_q(\mathbf{r})$, and the spin-orbit-current density $\nabla.\mathbf{J_q}(\mathbf{r})$, $(q = n, p)$.

The third model used for the density distribution is the deformed Fermi distribution, which will be used for Ne and

TABLE II. Same as Table I but for Mg isotopes.

Nucleus	R_n(fm)	R_p(fm)	R_m(fm)
^{20}Mg	2.445	2.900	2.727
^{21}Mg	2.511	2.900	2.740
^{22}Mg	2.574	2.900	2.757
^{23}Mg	2.634	2.900	2.776
^{24}Mg	2.692	2.900	2.798
^{25}Mg	2.747	2.900	2.822
^{26}Mg	2.801	2.900	2.847
^{27}Mg	2.852	2.900	2.874
^{28}Mg	2.902	2.900	2.901
^{29}Mg	2.950	2.900	2.930
^{30}Mg	2.997	2.900	2.959
^{31}Mg	3.042	2.900	2.988
^{32}Mg	3.087	2.900	3.018
^{33}Mg	3.130	2.900	3.048
^{34}Mg	3.172	2.900	3.079

TABLE III. Same as Table I but for oxygen isotopes.

Nucleus	R_n(fm)	R_p(fm)	R_m(fm)
^{16}O	2.445	2.592	2.519
^{17}O	2.511	2.592	2.549
^{18}O	2.574	2.592	2.582
^{19}O	2.634	2.592	2.616
^{20}O	2.692	2.592	2.652
^{21}O	2.747	2.592	2.689
^{22}O	2.801	2.592	2.726
^{23}O	2.852	2.592	2.764
^{24}O	2.902	2.592	2.802

Mg isotopes,

$$\rho_{i(=p,n)}(r,\theta) = \frac{\rho_{0i}}{1+\exp\left(\frac{r-R_i(\theta)}{a_i}\right)}, \tag{16}$$

where, the proton (neutron) half-density radius is written as,

$$R_i(\theta) = R_{0i}[1+\beta_{2i}Y_{20}(\theta)]. \tag{17}$$

To obtain the proton and neutron quadrupole deformation parameters, β_{2i}, half-density radii, R_{0i}, and diffuseness a_i we have performed RMF calculations in an axially symmetric deformed basis, using the relativistic mean-field Lagrangian density, adopting the force parameter NL3* [47,48]. Pairing correlations have been treated within the BCS method with constant gap approximation [48,49]. The results of the RMF quadrupole deformation parameters and root-mean-square (rms) radii are listed in Tables IV and V for Ne and Mg isotopes. Following Ref. [48], the quadrupole deformation parameters, appearing in the Fermi density, β_{2i} are fixed as calculated from the RMF theory, as listed in Tables IV and V. The other parameters of the deformed Fermi shape, the proton and neutron half-density radii and diffuseness are adjusted to reproduce the rms radii as predicted by the RMF calculations of Tables IV and V. A similar procedure has been used in Ref. [32], where the parameters of the harmonic oscillator density were determined by the RMF, adopting NL3* interaction.

TABLE IV. The calculated RMF neutron, proton, and matter radii and quadrupole deformation parameters of Ne isotopes.

Nucleus	R_n(fm)	R_p(fm)	R_m(fm)	β_{2n}	β_{2p}	β_{2m}
^{18}Ne	2.703	3.095	2.928	.047	0.155	0.107
^{19}Ne	2.845	3.077	2.969	0.071	0.144	0.110
^{20}Ne	2.927	3.042	2.985	0.076	0.129	0.103
^{21}Ne	3.001	3.003	3.002	0.436	0.423	0.430
^{22}Ne	3.048	2.966	3.011	0.451	0.422	0.438
^{23}Ne	3.081	2.926	3.014	0.375	0.359	0.368
^{24}Ne	3.091	2.880	3.005	0.225	0.237	0.230
^{25}Ne	3.140	2.854	3.029	0.119	0.131	0.123
^{26}Ne	3.210	2.846	3.075	0.037	0.040	0.038
^{27}Ne	3.283	2.852	3.133	0.116	0.132	0.122
^{28}Ne	3.346	2.877	3.186	0.129	0.161	0.141
^{29}Ne	3.394	2.890	3.229	0.051	0.069	0.057
^{30}Ne	3.446	2.908	3.276	0.013	0.008	0.012
^{31}Ne	3.554	2.924	3.364	0.184	0.177	0.182
^{32}Ne	3.638	2.972	3.444	0.382	0.346	0.371

TABLE V. Same as Table IV but for Mg isotopes.

Nucleus	R_n(fm)	R_p(fm)	R_m(fm)	β_{2n}	β_{2p}	β_{2m}
^{20}Mg	2.654	3.170	2.974	0.025	0.104	0.072
^{21}Mg	2.783	3.160	3.004	0.169	0.295	0.241
^{22}Mg	2.895	3.168	3.047	0.425	0.519	0.476
^{23}Mg	2.969	3.145	3.062	0.481	0.535	0.509
^{24}Mg	3.019	3.110	3.065	0.484	0.517	0.500
^{25}Mg	3.071	3.077	3.074	0.432	0.465	0.448
^{26}Mg	3.088	3.030	3.061	0.315	0.365	0.338
^{27}Mg	3.130	3.005	3.075	0.252	0.299	0.273
^{28}Mg	3.196	3.008	3.117	0.265	0.302	0.281
^{29}Mg	3.257	3.007	3.156	0.236	0.281	0.255
^{30}Mg	3.308	3.007	3.191	0.181	0.241	0.205
^{31}Mg	3.345	3.005	3.218	0.083	0.124	0.099
^{32}Mg	3.390	3.015	3.255	0.017	0.015	0.016
^{33}Mg	3.469	3.024	3.314	0.105	0.125	0.112
^{34}Mg	3.550	3.067	3.387	0.328	0.335	0.330
^{35}Mg	3.609	3.090	3.440	0.3948	0.383	0.390
^{36}Mg	3.663	3.111	3.489	0.442	0.415	0.433

As in Refs. [12,50] we perform an angle average over the polar angle θ,

$$\rho_{p,n}(r) = \frac{1}{2}\int_0^\pi \rho_{p,n}(r,\theta)\sin(\theta)d\theta. \tag{18}$$

It may be important to be noted that, the RMF theory has been successfully applied to study global properties of stable and unstable nuclei (see, for example, Refs. [47–49,51,52]). It has the advantage that it is providing a realistic self-consistent covariant relativistic description, based on meson theory, for nuclear structure. Thus taking RMF parameters and using them in a Fermi shape gives a simple description of the density distribution of stable and unstable nuclei under the constraint that its parameters predict realist radii.

III. RESULTS AND DISCUSSION

Figures 1–3 show the reaction cross sections of Ne, Mg, and O isotopes on ^{12}C calculated at around one GeV/nucleon using the Glauber model with the SP densities for both target and projectiles. For the target, ^{12}C, the predicted matter radius, using Eqs. (13)–(15), is found to be 2.41 fm, which seems to be reasonable in comparison with that deduced from electron scattering experiments [53]. The dash-dotted lines represent the free reaction cross sections calculated using Eqs. (1)–(9) for the free NN cross section (denoted by Free1), where, $F_{NN}(E,\rho) = F_{NN}(E,0)$. The solid lines represent calculations of the reaction cross sections defined by Eqs. (1)–(11), which include in-medium effects by the phenomenological model. The dashed lines, denoted by GP1, represent calculations of the reaction cross sections including in-medium NN cross sections as geometric effects of the Pauli operator, as described by Eq. (12) and using Eqs. (8) and (9) for the free NN cross section. Calculations using the

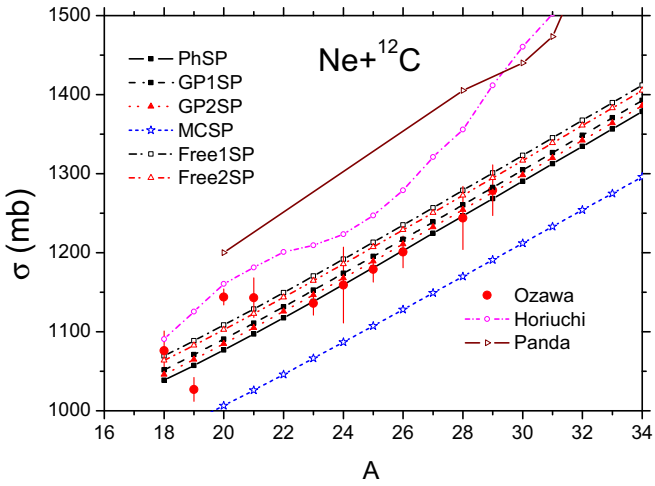

FIG. 1. The reaction cross sections of $^{18-32}$Ne + ^{12}C, calculated at about 1 GeV/u using the Glauber model with SP densities. The solid, dashed, dotted, and short-dotted lines (denoted by PhSP, GP1SP, GP2SP, and MCSP, respectively) represent the reaction cross sections calculated using the SP densities and the in-medium *NN* reaction cross sections described by the Ph, GP1, GP2, and MC models. The dash-dotted and dash-double dotted lines represent the calculation using the SP density and the free *NN* cross section as described by Eqs. (8) and (9) (Free1SP) and the that of the particle data group [30] (Free2SP). The calculations of Horiuchi *et al.* [11] and Panda *et al.* [12] around one GeV/u are shown for comparison. The experimental data are taken from Ozawa *et al.* [5].

GP model and the free *NN* cross sections of the particle data group [30] are shown in these figures by the dotted lines and denoted by GP2. The reaction cross section calculated without medium modifications and using the free *NN* cross section of [30] is shown by the dash double-dotted lines and denoted by Free2. The reaction cross sections calculated with medium modifications as described by the MC model is shown by the short dashed lines. The calculations of Horiuchi *et al.* [11],

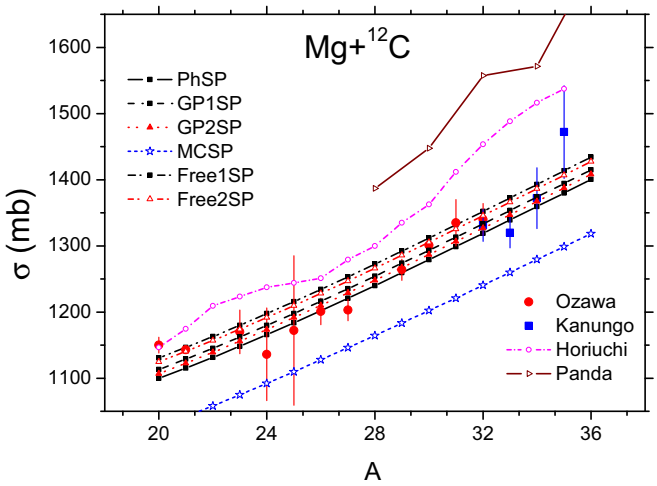

FIG. 2. Same as Fig. 1 but for $^{20-36}$Mg + ^{12}C. The experimental data are taken from Ozawa *et al.* [5] and Kanungo *et al.* [54].

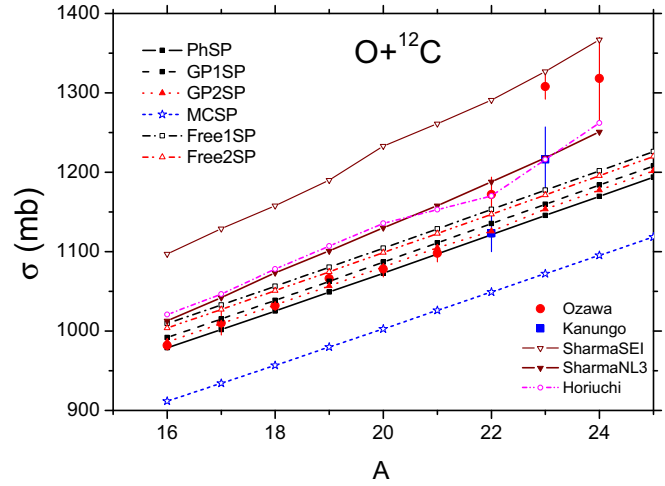

FIG. 3. Same as Fig. 1 but for $^{16-24}$O + ^{12}C. The calculation of Sharma *et al.* [13], which used the spherical SHF Skyrme force SKI-I and the RMF interaction NL3 are shown for comparison. The experimental data are taken from Ozawa *et al.* [5] and Kanungo *et al.* [55].

Panda *et al.* [12], and Sharma *et al.* [13] around one GeV/u are shown in these figures for comparison. The experimental data are taken from [5,54,55]. As shown from these figures calculations include in-medium *NN* cross sections through both the Ph and GP models, generally, reproduced the nucleus-nucleus reaction cross sections, where a good agreement is obtained, when the SP density distribution is used. The GP1 and GP2 models produce, slightly, larger nucleus-nucleus reaction cross sections than the Ph model. Both Ph and GP models reduced the reaction cross sections than the free models as expected. The MC model produces much lower reaction cross sections than the free and than the data. The calculations of Horiuchi *et al.* and Panda *et al.* neither predict the experimental cross sections nor the trend of data, where they predicted almost much larger reaction cross sections, as shown from Figs. 1–3. The nonrelativistic and relativistic calculations of Sharma *et al.* [13] of the reaction of oxygen isotopes overestimated the date as shown for Fig. 3. In Fig. 4 we show calculations of the reaction cross sections of oxygen isotopes on ^{12}C, as in Fig. 3, but using SHF density with SKRA parametrization instead of the SP density. As shown from this figure the SHF density, which is more realistic than the SP density, produced much larger reaction cross sections even including medium effects through the Ph and GP models. On the other hand, the SP density, which generally reproduced the reaction cross section data predicted, in general, smaller radii, as seen in Tables I–III. For example, the matter radii of ^{20}Ne, ^{24}Mg, and ^{16}O predicted by the SP model density are 2.665, 2.798, and 2.519 fm, respectively, as seen from Tables I–III, while that predicted by the RMF calculations, employing NL3* interaction, for ^{20}Ne and ^{24}Mg, are 2.985 and 3.065 fm, as seen from Tables IV and V, respectively. For ^{16}O electron scattering experiments give the value 2.7 fm [53]. A similar remark has been noticed recently in Ref. [32] for the case of the reactions of oxygen isotopes with ^{12}C, where

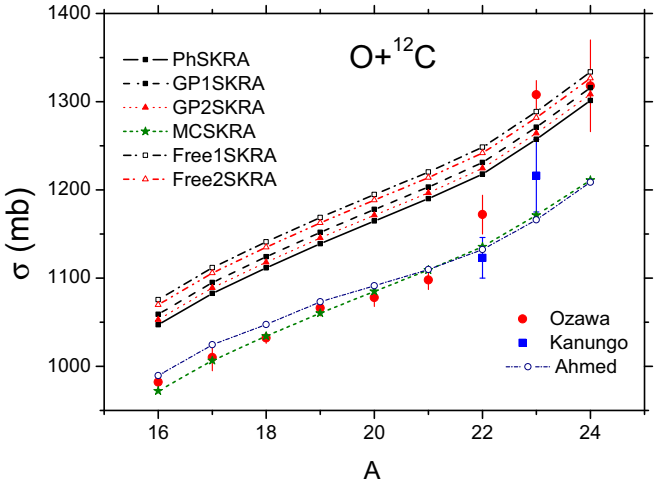

FIG. 4. Same as Fig. 3 but calculated using the density distributions derived from SHF calculation using SKRA parametrization. The calculations Ahmed *et al.* [32] are shown for comparison.

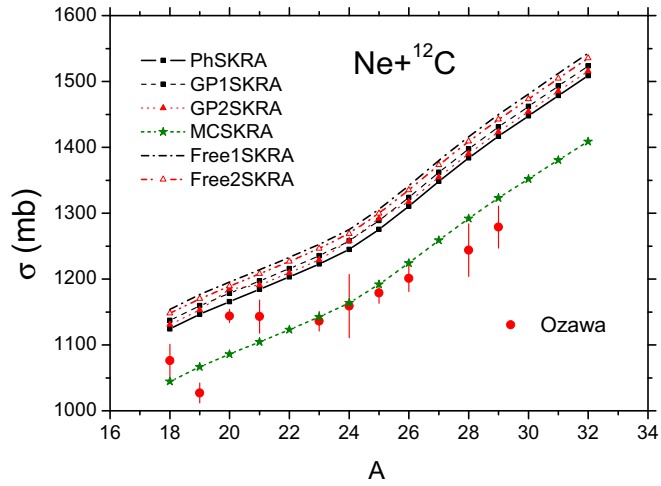

FIG. 5. Same as Fig. 4 but for $^{18-32}$Ne + ^{12}C.

they used Slater determinants of harmonic oscillator single-particle wave functions (SDHO) to describe the densities of oxygen isotopes. They found that the radii deduced from the reaction cross section data, using SDHO densities are much smaller as compared to those obtained using RMF densities. For example, for ^{16}O the deduced matter radius has been found to be 2.55 fm, similar to that predicted by the SP model namely; 2.52 fm, which is smaller than that of the electron scattering data or RMF $\backsimeq$ 2.72 fm [32]. In order to describe the data with the correct realistic radii, they readjusted the harmonic oscillator parameters of the density distributions to reproduce the RMF radii and modified the in-medium *NN* amplitude at one GeV by considering the effects arising due to phase variation, higher momentum transfer components, and Pauli blocking. With these modifications they are able to reproduce the data for $^{16-24}$O + ^{12}C except for ^{23,24}O. In this work, we used this MC model for the *NN* cross section in the calculations of the nucleus-nucleus reaction cross sections and using realistic SHF densities for both target and projectiles adopting SKRA interaction. The result of these modified and more realistic calculations is shown in Fig. 4 by the short-dashed line. Also shown in Fig. 4 the calculations of Ahemd *et al.* [32] for comparison. As shown from this figure the data are satisfactorily described even better than that of Ahmed *et al.*, especially for lighter isotopes, where they used modified harmonic oscillator densities, while densities derived from SHF calculation are used here.

Figure 5 is the same as Fig. 1 but SHF densities are used in the calculation of the reaction cross sections instead of the SP densities. Again the MC model for the *NN* cross, which reduces the reaction cross section much more than the other in-medium Ph, GP1, and GP2 models, generally, described the data. However, the data are not satisfactorily described, such as in the case of oxygen isotopes, which are predicted, in general, to be spherical. This is due to the fact that most of the Ne and Mg isotopes are predicted to be deformed, as seen from Tables IV and V.

Figures 6 and 7 show the reaction cross sections of Ne and Mg isotopes as Figs. 1 and 2 but calculated using the angle-averaged deformed Fermi density, as described in Sec. II B where the deformation parameters and rms radii of the DF density are described by the RMF model with NL3* interaction, as listed in Tables IV and V. The data are satisfactorily described when using MC model for the *NN* cross section with deformed Fermi density, which has realistic radii. The cross sections calculated using DF density and the in-medium phenomenological and geometrical Pauli, as well as free models, overestimated the data. The reason that Ph and GP models produce larger reaction cross sections than the MC model is that the MC model considers besides the Pauli blocking effects, which have also been considered in both Ph and GP models, other effects of medium modifications arising from phase variation, and higher momentum transfer components, which additionally, reduce the reaction cross sections.

Finally, it is important to compare the results of the present reaction cross section calculations within the Glauber model at 1 GeV with that of our previous work [14] at intermediate

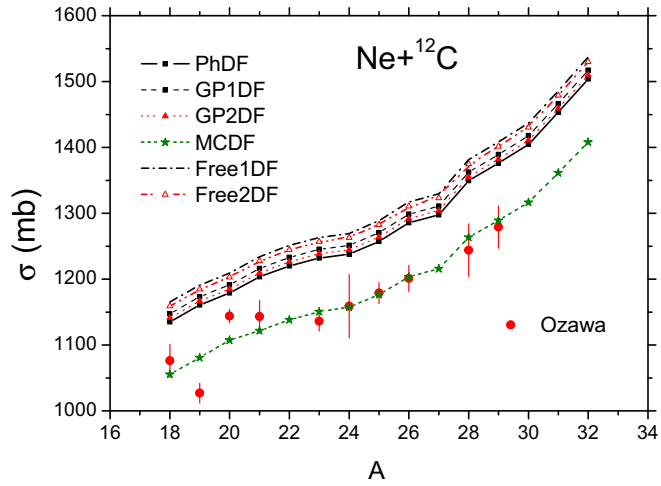

FIG. 6. Same as Fig. 5 but calculated using the DF density.

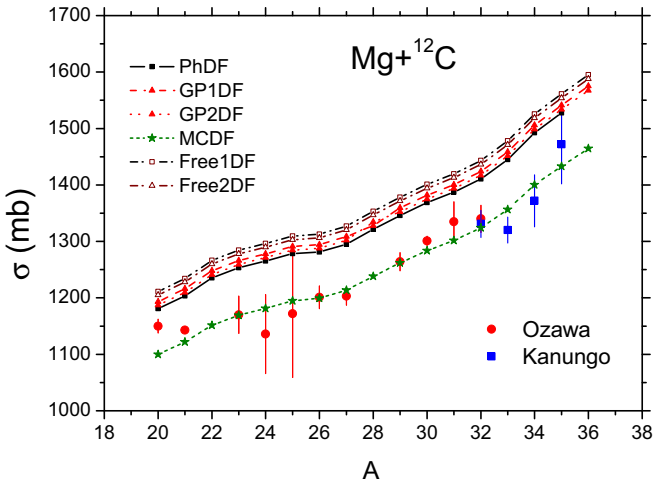

FIG. 7. Same as Fig. 5 but for $^{20-36}$Mg + ^{12}C.

energy. We found that both the Ph and GP models, which satisfactorily described the data at 240 MeV/u with realistic densities cannot do the same at high energy around 1 GeV. In fact, the phenomenological model is a modification of the parametrization of *NN* cross section derived from the relativistic *G* matrix at intermediate energy. The geometrical Pauli model is a simple geometrical treatment of the angle-averaged Pauli blocking operator appearing in the Brueckner *G* matrix, which is normally solved at energies less than 300 MeV/u, due to pion production threshold. Therefore these two models could be more appropriate to intermediate-energy nuclear collisions but they could need further modifications in order to also well work at high energy. However, further investigations of medium modifications models for other different reactions at high energy is required. The work along this direction is underway.

IV. SUMMARY AND CONCLUSION

We studied the effects of in-medium *NN* cross sections and nuclear densities on the reaction cross sections of neon, magnesium, and oxygen isotopes colliding by ^{12}C target at 1.0 GeV/nucleon, in the framework of the Glauber model. In-medium effects are included through three different *NN* cross section models; the phenomenological, geometrical Pauli, and the modified combined. The latter involves combined effects arising due to phase variation, higher momentum transfer components, and Pauli blocking. For the density distributions, we used the SP, SHF, and DF densities. The deformation parameters and radii of the deformed Fermi density are determined by RMF calculation. The Saw Pauli density produces smaller rms radii than the realistic SHF and RMF densities. The in-medium modifications are important, where they, in general, reduce the reaction cross section. The Ph and GP models, which include Pauli blocking effect, reduce the cross sections by about 30 mb at all energies, depending on the model but overestimated the reaction cross section data when using realistic densities. The data can be reproduced using realistic densities and the MC model for medium modifications, which include, besides Pauli blocking, the effects arising from phase variation and higher momentum transfer components, which additionally reduce the reaction cross sections, and they are not considered in the Ph and GP models.

[1] I. Tanihata *et al.*, Phys. Lett. B **160**, 380 (1985); Phys. Rev. Lett. **55**, 2676 (1985).
[2] W. Mittig *et al.*, Phys. Rev. Lett. **59**, 1889 (1987).
[3] R. E. Warner *et al.*, Phys. Rev. C **52**, R1166(R) (1995).
[4] D. Q. Fang *et al.*, Phys. Rev. C **61**, 064311 (2000).
[5] A. Ozawa *et al.*, Nucl. Phys. A **691**, 599 (2001); A. Ozawa, T. Suzuki, and I. Tanihata, *ibid.* **693**, 32 (2001).
[6] R. E. Warner, I. J. Thompson, and J. A. Tostevin, Phys. Rev. C **65**, 044617 (2002).
[7] M. Takechi *et al.*, Mod. Phys. Lett. A **25**, 1878 (2010).
[8] T. Nakamura *et al.*, Phys. Rev. Lett. **103**, 262501 (2009).
[9] W. Horiuchi, Y. Suzuki, P. Capel, and D. Baye, Phys. Rev. C **81**, 024606 (2010).
[10] K. Minomo, T. Sumi, M. Kimura, K. Ogata, Y. R. Shimizu, and M. Yahiro, Phys. Rev. Lett. **108**, 052503 (2012).
[11] W. Horiuchi, T. Inakura, T. Nakatsukasa, and Y. Suzuki, Phys. Rev. C **86**, 024614 (2012).
[12] R. N. Panda, Mahesh K. Sharma, and S. K. Patra, Mod. Phys. Lett. A **29**, 1450013 (2014).
[13] M. K. Sharma, R. N. Panda, M. K. Sharma, and S. K. Patra, Braz. J. Phys. **45**, 138 (2015).
[14] M. Rashdan, Eur. Phys. J. A **50**, 141 (2014).
[15] D. Alonso and F. Sammarruca, Phys. Rev. C **67**, 054301 (2003).
[16] E. van Dalen, C. Fuchs, and A. Faessler, Nucl. Phys. A **744**, 227 (2004); Eur. Phys. J. A **31**, 29 (2007).
[17] E. N. E. van Dalen and H. Müther, Phys. Rev. C **82**, 014319 (2010); E. N. E. vanDalen and H. Muther, Int. J. Mod. Phys. E **19**, 2077 (2010).
[18] N. van Giai, B. V. Carlson, Z. Ma, and H. H. Wolter, J. Phys. G **37**, 064043 (2010).
[19] H. Müther, R. Machleidt, and R. Brockmann, Phys. Rev. C **42**, 1981 (1990).
[20] P. Gogelein, E. N. E. van Dalen, C. Fuchs, and H. Müther, Phys. Rev C **77**, 025802 (2008).
[21] R. Machleidt, Adv. Nucl. Phys. **19**, 189 (1989).
[22] H. Muether and A. Polls, Prog. Part. Nucl. Phys. **45**, 243 (2000).
[23] R. Brockman and R. Machleidt, Phys. Lett. B **149**, 283 (1984); R. Machleidt and R. Brockman, *ibid.* **160**, 364 (1985).
[24] N. Ohtsuka, M. Shabshiry, R. Linden, H. Müther, and A. Faessler, Nucl. Phys. A **490**, 715 (1988).
[25] R. Xu, Z. Ma, E. N. E. van Dalen, and H. Müther, Phys. Rev. C **85**, 034613 (2012); M. Hemalatha, Y. K. Gambhir, S. Kailas, and W. Haider, *ibid.* **75**, 037602 (2007).
[26] W. Zou, Y. Tian, and Z.-Y. Ma, Phys. Rev. C **78**, 064613 (2008); R. Xu *et al.*, EPJ Web Conf. **146**, 12009 (2017).
[27] G. Q. Li and R. Machleidt, Phys. Rev. C **48**, 1702 (1993).

[28] G. Q. Li and R. Machleidt, Phys. Rev. C **49**, 566 (1994).
[29] C. Xiangzhou, F. Jun, S. Wenqing, M. Yugang, W. Jiansong, and Y. Wei, Phys. Rev. C **58**, 572 (1998).
[30] M. Karakoc and C. Bertulani, 11th International Conference on Nucleus-Nucleus Collisions (NN2012); J. Phys.: Conf. Ser. **420**, 012074 (2013); C. A. Bertulani and C. De Conti, Phys. Rev. C **81**, 064603 (2010); B. Chen, F. Sammarruca, and C. A. Bertulani, *ibid.* **87**, 054616 (2013); B. Chen, F. Sammarruca, and C. A. Bertulani (Particle Data Group), J. Phys. G **33**, 1 (2006).
[31] S. K. Charagi and S. K. Gupta, Phys. Rev. C **41**, 1610 (1990).
[32] S. Ahmad, A. A. Usmani, Shakeb Ahmad, and Z. A. Khan, Phys. Rev. C **95**, 054601 (2017).
[33] L. C. Chamon, B. V. Carlson, L. R. Gasques, D. Pereira, C. De Conti, M. A. G. Alvarez, M. S. Hussein, M. A. Candido Ribeiro, E. S. Rossi, and C. P. Silva, Phys. Rev. C **66**, 014610 (2002).
[34] D. Vautherin and D. M. Brink, Phys. Rev. C **5**, 626 (1972).
[35] L. W. Neise, J. Maruhn, and W. Greiner, Z. Phys. A **323**, 195 (1986).
[36] M. Rashdan, Mod. Phys. Lett. A **15**, 1287 (2000).
[37] A. Kohama, K. Iida, and K. Oyamatsu, Phys. Rev. C **78**, 061601(R) (2008).
[38] Y. Togano *et al.*, Phys. Lett. B **761**, 412 (2016)
[39] M. Takechi *et al.*, Phys. Rev. C **90**, 061305 (2014).
[40] D. Chauhan, Z. A. Khan, and A. A. Usmani, Phys. Rev. C **90**, 024603 (2014).
[41] K. Tanaka *et al.*, Phys. Rev. Lett. B **104**, 062701 (2010).
[42] S. Ahmad, D. Chauhan, A. A. Usmani, and Z. A. Khan, Eur. Phys. J. A **52**, 128 (2016).
[43] Q. Li, Z. Li, S. Soff, M. Bleicher, and H. Stoecker, J. Phys. G **32**, 407 (2006).
[44] A. de Vismes, P. Roussel-Chomaz, and F. Carstoiu, Phys. Rev. C **62**, 064612 (2000).
[45] N. Marimuthu, V. Singh, and S. S. R. Inbanathan, Adv. High Energy Phys. **2017**, 7907858 (2017).
[46] N. Marimuthu, V. Singh, and S. S. R. Inbanathan, Indian J. Phys. **91**, 431 (2017).
[47] G. A. Lalazissis *et al.*, Phys. Lett. B **671**, 36 (2009).
[48] M. Rashdan, Phys. Rev. C **86**, 044610 (2012); Int. J. Mod. Phys. E **21**, 2106 (2012).
[49] A. Karim and S. Ahmad, Phys. Rev. C **92**, 064608 (2015).
[50] K. Minomo *et al.*, Phys. Rev. C **84**, 034602 (2011).
[51] M. Bender, P. Heenen, and P. G. Reinhard, Rev. Mod. Phys. **75**, 121 (2003).
[52] L. S. Geng, H. Toki, and J. Meng, Prog. Theor. Phys. **112**, 603 (2004); **113**, 785 (2005).
[53] H. de Vries, C. W. de Jager, and C. de Vries, Adndt **36**, 495536 (1987).
[54] R. Kanungo *et al.*, Phys. Rev. C **83**, 021302(R) (2011).
[55] R. Kanungo *et al.*, Phys. Rev. C **84**, 061304(R) (2011).